International Journal of Mechanical Sciences 77 (2013) 194–204

Contents lists available at ScienceDirect

International Journal of Mechanical Sciences

journal homepage: www.elsevier.com/locate/ijmecsci

Evaluating the significance of hardening behavior and unloading modulus under strain reversal in sheet springback prediction

Shun-lai Zang [a,*], Myoung-gyu Lee [b], Ji Hoon Kim [c]

[a] School of Mechanical Engineering, Xi'an Jiaotong University, No. 28, Xianning Road, Xi'an, Shaanxi, China
[b] Graduate Institute of Ferrous Technology, Pohang University of Science and Technology, San 31, Hyoja-dong, Nam-gu, Pohang, Geongbuk 790-784, Republic of Korea
[c] Materials Deformation Department, Korea Institute of Materials Science, 797 Changwon-daero, Changwon, Gyeongnam 642-831, Republic of Korea

ARTICLE INFO

Article history:
Received 13 October 2012
Received in revised form
8 June 2013
Accepted 30 September 2013
Available online 14 October 2013

Keywords:
Bauschinger effect
Transient behavior
Permanent softening
Young's modulus
Springback prediction

ABSTRACT

Springback is one of the most important problems that should be compensated in sheet metal forming process with the increasing application of advanced high strength steels and light-weight alloys. In the finite element analyses for the springback, accurate modeling of Bauschinger effect, transient behavior and permanent softening under cyclic loading has been recognized as the most critical hardening behavior in the constitutive modeling aspect. However, if parts of these hardening behavior are not well modelled, is the accuracy of springback prediction seriously deteriorated? To answer this question, in this paper the significance of Bauschinger effect and transient behavior, permanent softening and unloading modulus in springback prediction were estimated using the springback problem of U-draw/bending simulations proposed at Numisheet2011 Benchmark. A recent anisotropic non-linear kinematic (ANK) model [Zang S, Guo C, Thuillier S, Lee M. A model of one-surface cyclic plasticity and its application to springback prediction. Int J Mech Sci 2011;53:425–35.] was adopted to estimate the significance of hardening behavior and unloading modulus because of its special feature. The ANK model can predict exactly the same monotonous stress–strain curves for different hardening schemes, while different Bauschinger effect and transient behavior under one-dimensional cyclic loading can be also modelled. This feature is quite suitable to quantitatively evaluate the effects of the aforementioned hardening behaviors in springback prediction. Initial anisotropy is described by the anisotropic yield function Yld2000-2d. The unloading behavior is also considered by defining Young's modulus as a function of equivalent plastic strain. Several quantitative analyses were carried out to distinguish the effect of each hardening component and unloading elastic modulus scheme. Finally, the predicted springback by different models were compared with experiments for both as-received and pre-strained DP780 steel sheets.

1. Introduction

Nowadays, numerous works have been done to obtain reliable simulation results in predicting springback of sheet metals [1–4]. Since the deformation of a sheet during forming is very complex, the accuracy of simulation is greatly influenced by many important factors. Constitutive model, which describes the mechanical behavior of materials, has been considered as one of the most important factors and paid more and more attentions during the past decades [5–10].

Without doubt, the accuracy of springback prediction will be enhanced when all kinds of the mechanical behavior could be accurately described. But, if the constitutive model cannot capture all of them at the same time, which component of the mechanical behavior should be priorly modelled in springback prediction so that the accuracy is not much deteriorated? This question is reasonable because most of the recently proposed advanced constitutive models might not predict actual mechanical behavior observed in experiments due to the complexity of materials. Moreover, most advanced constitutive models are not always available in commercial finite element packages [11,12] which are being widely used in engineering applications. Consequently, the study on the significance of each mechanical behavior that can be selectively reflected in the constitutive model is required.

In particular, the mechanical behavior of materials under cyclic loading has gained more interests since the strain reversal is common in sheet metal forming process. Fig. 1 shows a typical flow stress curve of outer material (in the thickness direction) when the sheet flows into die shoulder. The Bauschinger effect and transient behavior are defined as an early re-yielding and

* Corresponding author. Tel.: +86 29 82668607x806; fax: +86 29 82668607x806.
E-mail addresses: shawn@mail.xjtu.edu.cn, shunlai.zang@gmail.com (S.-l. Zang).

0020-7403/$ - see front matter © 2013 Elsevier Ltd. All rights reserved.
http://dx.doi.org/10.1016/j.ijmecsci.2013.09.033

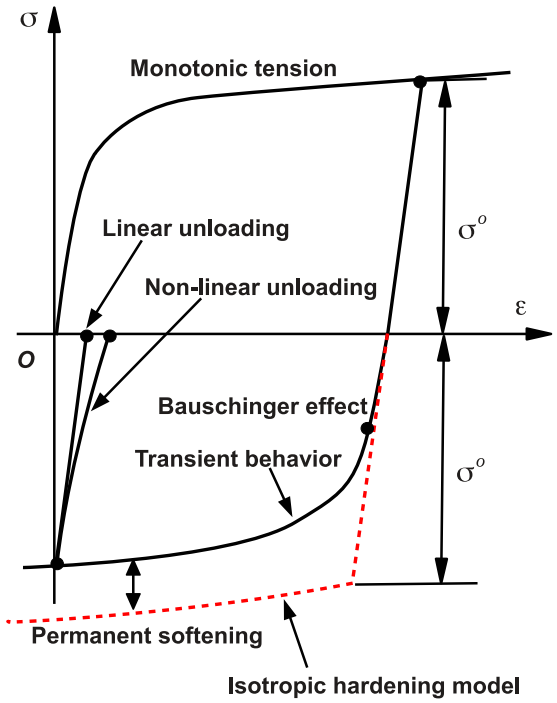

Fig. 1. A schematic unloading curve under reverse loading to illustrate the Bauschinger effect, transient behavior, permanent softening and non-linear unloading modulus.

subsequent rapid change of hardening rate at the beginning of reversal loading, respectively [13–15]. The permanent softening is either absent for some materials [16] or exists as a stress offset between monotonous and reversed flow stresses [16–18]. As for the unloading behavior, its non-linear nature has been well recognized [15,19,20]. To capture it, an unloading modulus as a function of plastic strain is usually adopted in springback prediction [2,21].

As already known, the amount of springback depends on two important aspects, i.e., the stress level in material before unloading and unloading modulus [3,4]. If the stress state is not located in the strain range of Bauschinger effect and transient behavior under reverse loading, similar springback should be predicted. Although many hardening models have been evaluated [2,9,18,22–25], the above speculation is seldom mentioned and still unclear. The reason is that it is challenging to maintain the overall mechanical behavior, while the Bauschinger effect and transient behavior are varied in numerical simulation. This is essential to perform an efficient sensitivity analysis to evaluate the significance of several important features in materials.

The main objective of this study is to quantitatively estimate the significance of constitutive behavior. Among them, the Bauschinger effect, transient behavior, permanent softening and unloading modulus were chosen as main factors that influence in the prediction of springback. For this purpose, recently proposed isotropic-kinematic hardening model, namely ANK model, was employed [25]. Here, the term ANK model refers to the combined hardening model, which includes both the isotropic hardening law and the kinematic hardening model. In Section 2, the ANK model [25] is briefly reviewed and its special feature in modeling of Bauschinger effect and transient behavior is explained. In Section 3, the 2D U-draw/bending springback problem presented in the Numisheet2011 benchmark report [26] is summarized, which is chosen as the example of springback analysis. Finally, in Section 4 a detailed analysis on the influences of hardening and unloading behavior on the springback prediction is discussed.

2. Theory

2.1. Review on the ANK model

Since the present work utilizes the special feature of the ANK model, a brief review on the ANK model is provided in this subsection [25]. Regarding the special feature, it will be explained in the following Section 2.2. For any combined isotropic-kinematic hardening model, the consistency condition, which is addressed in Chung's recent work [27], should be satisfied. It will be seen that the present ANK model is the Ziegler type-based kinematic hardening model, thus the consistency condition is confirmed.

For a combined isotropic-kinematic hardening model, the equivalent stress is usually defined as

$$\overline{\sigma} = f(\boldsymbol{\sigma} - \boldsymbol{\alpha}) \tag{1}$$

where f is the yield function, $\boldsymbol{\sigma}$ is the Cauchy stress tensor and $\boldsymbol{\alpha}$ is the backstress tensor, which defines the central position of the current yield surface (initially, it is usually assumed to be zero). $\overline{\sigma}$ measures the size of the yield surface as a first order homogeneous function.

According to the associated flow rule, plastic strain rate is

$$\dot{\boldsymbol{\varepsilon}}^p = \dot{\lambda}\frac{\partial f}{\partial \boldsymbol{\sigma}} \tag{2}$$

where $\dot{\lambda}$ is the plastic multiplier.

The plastic work rate is defined as

$$\dot{w}^p = (\boldsymbol{\sigma} - \boldsymbol{\alpha}) : \dot{\boldsymbol{\varepsilon}}^p = \overline{\sigma}\,\dot{\bar{\varepsilon}}^p \tag{3}$$

where $\dot{\bar{\varepsilon}}^p$ is the equivalent plastic strain rate.

Using Euler's theorem for the homogeneous function f

$$(\boldsymbol{\sigma} - \boldsymbol{\alpha}) : \frac{\partial f}{\partial \boldsymbol{\sigma}} = \overline{\sigma} \tag{4}$$

Substituting Eq. (2) into Eq. (3), and combining with Eq. (4), the equivalent plastic strain rate can be written as

$$\dot{\bar{\varepsilon}}^p = \dot{\lambda} \tag{5}$$

With the assumption of small elastic and large plastic deformation, strain rate $\dot{\boldsymbol{\varepsilon}}$ can be decomposed into an elastic component $\dot{\boldsymbol{\varepsilon}}^e$ and a plastic component $\dot{\boldsymbol{\varepsilon}}^p$. For isotropic elasticity, the generalized Hooke's law states that Cauchy stress tensor is proportional to elastic strain tensor, i.e.,

$$\dot{\boldsymbol{\sigma}} = \mathbf{C}^e : \dot{\boldsymbol{\varepsilon}}^e = \mathbf{C}^e : (\dot{\boldsymbol{\varepsilon}} - \dot{\boldsymbol{\varepsilon}}^p) \tag{6}$$

where $\mathbf{C}^e$ is fourth-order elasticity tensor.

In the ANK model [25], a two-term kinematic hardening model is used therefore the backstress $\boldsymbol{\alpha}$ can be written as

$$\boldsymbol{\alpha} = \boldsymbol{\alpha}_1 + \boldsymbol{\alpha}_2 \tag{7}$$

where α_1 is a non-linear Chaboche kinematic hardening model, α_2 is a linear Ziegler model. Then, the evolution of backstresses can be respectively defined as

$$\dot{\boldsymbol{\alpha}}_1 = \frac{C_1}{\overline{\sigma}}(\boldsymbol{\sigma} - \boldsymbol{\alpha})\dot{\bar{\varepsilon}}^p - \gamma_1 \boldsymbol{\alpha}_1 \dot{\bar{\varepsilon}}^p \tag{8a}$$

$$\dot{\boldsymbol{\alpha}}_2 = \frac{C_2}{\overline{\sigma}}(\boldsymbol{\sigma} - \boldsymbol{\alpha})\dot{\bar{\varepsilon}}^p \tag{8b}$$

where C_1, γ_1 and C_2 are material hardening parameters.

Considering the yield criterion F, the plastic deformation can be determined when $F=0$, i.e.,

$$F = f(\boldsymbol{\sigma} - \boldsymbol{\alpha}) - \sigma^{\circ} = 0 \tag{9}$$

where σ° is the current flow stress. To generate a relative flat stress–strain curve, a modified isotropic hardening model was

used for σ° in the ANK model [25]

$$\sigma^{\circ} = \sigma_{\circ} + R_{iso} = \sigma_{\circ} + Q(1-e^{-b\bar{\varepsilon}^p}) - \frac{C_1}{\gamma_1}(1-e^{-\gamma_1\bar{\varepsilon}^p}) \tag{10}$$

where $\sigma_{\circ}$ represents the initial yield stress, R_{iso} is the isotropic hardening, and $\bar{\varepsilon}^p$ is the equivalent plastic strain. C_1 and γ_1 are the same as the parameters in Eq. (8a). Q and b are material hardening parameters.

During plastic deformation, the Cauchy stress should stay on the yield surface all the time, which leads to the consistency condition for the yield criterion F,

$$\dot{F} = \frac{\partial f}{\partial \boldsymbol{\sigma}} : (\dot{\boldsymbol{\sigma}} - \dot{\boldsymbol{\alpha}}) - \frac{d\sigma^{\circ}}{d\bar{\varepsilon}^p}\dot{\bar{\varepsilon}}^p = 0 \tag{11}$$

Substituting Eqs. (2), (5), (6) and (8) into Eq. (11), after some manipulations,

$$\dot{\lambda} = \frac{\dfrac{\partial f}{\partial \boldsymbol{\sigma}} : \boldsymbol{C}^{\boldsymbol{e}} : \dot{\boldsymbol{\varepsilon}}}{\dfrac{\partial f}{\partial \boldsymbol{\sigma}} : \boldsymbol{C}^{\boldsymbol{e}} : \dfrac{\partial f}{\partial \boldsymbol{\sigma}} + A_{kin} + A_{iso}} \tag{12}$$

where A_{iso} is equal to $d\sigma^{\circ}/d\bar{\varepsilon}^p$, A_{kin} is

$$A_{kin} = \frac{\partial f}{\partial \boldsymbol{\sigma}} : \left[\frac{C_1 + C_2}{\bar{\sigma}}(\boldsymbol{\sigma} - \boldsymbol{\alpha}) - \gamma_1 \boldsymbol{\alpha}_1\right] \tag{13}$$

The standard tangent modular can be obtained by substitution of Eq. (12) back into Eq. (6):

$$\dot{\boldsymbol{\sigma}} = \boldsymbol{C}^{ep} : \dot{\boldsymbol{\varepsilon}} \tag{14}$$

where $\boldsymbol{C}^{ep}$ is the standard tangent modular tensor, which can be written as

$$\boldsymbol{C}^{ep} = \boldsymbol{C}^{\boldsymbol{e}} - \frac{\left(\boldsymbol{C}^{\boldsymbol{e}} : \dfrac{\partial f}{\partial \boldsymbol{\sigma}}\right) \otimes \left(\boldsymbol{C}^{\boldsymbol{e}} : \dfrac{\partial f}{\partial \boldsymbol{\sigma}}\right)}{\dfrac{\partial f}{\partial \boldsymbol{\sigma}} : \boldsymbol{C}^{\boldsymbol{e}} : \dfrac{\partial f}{\partial \boldsymbol{\sigma}} + A_{kin} + A_{iso}} \tag{15}$$

2.2. Special feature in modeling of Bauschinger effect and transient behavior

In this subsection, the special feature of the ANK model [25] in modeling of Bauschinger effect and transient behavior is explained. Here, the special feature does not refer to the capability of hardening model in capturing the Bauschinger effect, transient behavior and permanent softening as the works [28–32]. The special feature is that, during monotonic loading, the ANK model produces exactly the same uni-axial plastic flow stress curve. Under strain reversal, different Bauschinger effects and transient behavior are simulated. It is important in the sensitivity analysis because the variables should be kept except those which are investigating. As already mentioned, the ANK model is a combined isotropic-kinematic hardening model based on two components nonlinear kinematic hardening scheme. For the kinematic hardening model, the backstress is decomposed into two parts; i.e., a linear Ziegler term [33] is used to capture the permanent softening as explained in the literature [25] and a non-linear standard Chaboche model [34] is employed to capture the Bauschinger effect and transient behavior. Note that the Ziegler type linear kinematic hardening model was originally introduced to account for the Bauschinger effect but it was found to have permanent softening as well [33]. So the non-linear Chaboche kinematic hardening model was introduced to have the Bauschinger effect and transient behavior only without permanent softening [34]. As for the isotropic hardening model, it involves five material parameters, $\sigma_{\circ}$, Q, b, C_1 and γ_1, as shown in Eq. (10). Here, the last two parameters, C_1 and γ_1, are same as those of backstress α_1. As already known, the integral equation of backstress α_1 under uni-axial tension is exactly identical to the last term of Eq. (10). Therefore, the predicted flow stress under uni-axial tension is irrelevant to the parameters C_1 and γ_1 since the flow stress is equal to the sum of kinematic and isotropic hardening equations. The following paragraphs conduct an analytical deduction on the ANK model under uni-axial loading to better understand its predicted forward and reverse flow stresses.

In uni-axial tension along rolling direction, the predicted forward flow stress can be calculated from

$$\sigma_{forward} = \sigma_{\circ} + R_{iso} + \alpha^f_{ANK} \tag{16}$$

where α^f_{ANK} stands for the backstress in forward uni-axial loading. Although the backstress is tensor, there is only one non-zero component for the ANK model in the case of uni-axial tension along rolling direction.

Integrating Eq. (8), the backstress α^f_{ANK} can be written as

$$\alpha^f_{ANK} = \frac{C_1}{\gamma_1}(1-e^{-\gamma_1\bar{\varepsilon}^p}) + C_2\bar{\varepsilon}^p \tag{17}$$

Substituting Eqs. (17) and (10) into Eq. (16), the flow stress of uni-axial tension can be obtained

$$\sigma_{forward} = \sigma_{\circ} + Q(1-e^{-b\bar{\varepsilon}^p}) + C_2\bar{\varepsilon}^p \tag{18}$$

Since the non-linear kinematic hardening model α_1 in the ANK model [25] is used to capture the Bauschinger effect and transient behavior, the above $\sigma_{forward}$ indicates that the forward flow stress in uni-axial tension is independent to the material parameters of backstress α_1. Supposing the equivalent plastic strain before strain reversal is $\bar{\varepsilon}^p_*$, the predicted reverse flow stress $\sigma_{reverse}$ can be calculated from

$$\sigma_{reverse} = -\sigma_{\circ} - R_{iso} + \alpha^r_{ANK} \quad \text{with} \quad \bar{\varepsilon}^p > \bar{\varepsilon}^p_* \tag{19}$$

where α^r_{ANK} represents the backstress under reverse uni-axial loading. Similarly, there is only one non-zero component for the backstress in the case of uni-axial compression along rolling direction. Considering the change of loading direction and the continuity of backstress, α^r_{ANK} can be integrated from Eqs. (8)

$$\alpha^r_{ANK} = -\frac{C_1}{\gamma_1}(1-2e^{-\gamma_1(\bar{\varepsilon}^p-\bar{\varepsilon}^p_*)} + e^{-\gamma_1\bar{\varepsilon}^p}) - C_2(\bar{\varepsilon}^p - 2\bar{\varepsilon}^p_*) \quad \text{with } \bar{\varepsilon}^p > \bar{\varepsilon}^p_* \tag{20}$$

Substituting Eqs. (20) and (10) into Eq. (19), the predicted flow stress during reverse loading can be obtained

$$\sigma_{reverse} = -\sigma_{\circ} - Q(1-e^{-b\bar{\varepsilon}^p}) - C_2\bar{\varepsilon}^p + \frac{2C_1}{\gamma_1}(e^{-\gamma_1(\bar{\varepsilon}^p-\bar{\varepsilon}^p_*)} - e^{-\gamma_1\bar{\varepsilon}^p}) + 2C_2\bar{\varepsilon}^p_* \quad \text{with } \bar{\varepsilon}^p > \bar{\varepsilon}^p_* \tag{21}$$

Comparing Eqs. (18) and (21), it can be seen that the absolute value of the first three terms of Eq. (21) is equal to that of Eq. (18), but opposite in sign. If we subtract the absolute value of Eq. (21) from Eq. (18), the following relationship can be obtained:

$$\Delta\sigma = |\sigma_{forward}| - |\sigma_{reverse}| = \frac{2C_1}{\gamma_1}(e^{-\gamma_1(\bar{\varepsilon}^p-\bar{\varepsilon}^p_*)} - e^{-\gamma_1\bar{\varepsilon}^p}) + 2C_2\bar{\varepsilon}^p_* \tag{22}$$

where $\Delta\sigma$ is the gap between forward and reverse flow stresses, which represents the Bauschinger effect, transient behavior and permanent softening. The gap between the flow stress at the start of unloading σ_f and the initial yield stress during reverse loading σ_r is usually defined as the amount of the Bauschinger effect. Then the predicted amount of the Bauschinger effect $\Delta\sigma_{bauschinger}$ can be defined by assuming $\bar{\varepsilon}^p = \bar{\varepsilon}^p_*$ in Eq. (22).

$$\Delta\sigma_{bauschinger} = \sigma_f - \sigma_r = \frac{2C_1}{\gamma_1}(1-e^{-\gamma_1\bar{\varepsilon}^p_*}) + 2C_2\bar{\varepsilon}^p_* \tag{23}$$

It can be seen from Eq. (23) that the amount of the Bauschinger effect depends on the plastic deformation before unloading, $\bar{\varepsilon}^p_*$, and three material parameters, C_1, γ_1 and C_2.

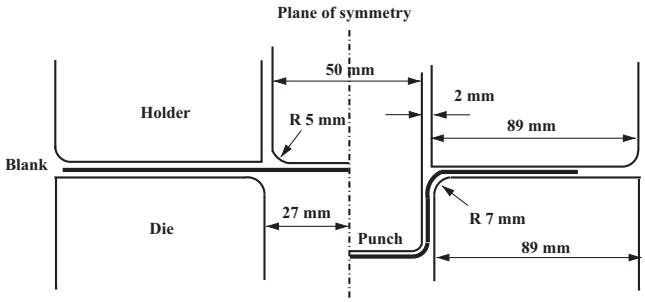

Fig. 2. A schematic view of tools and dimensions for U-draw/bending test.

3. U-draw/bending springback problem

In the present work, the 2D U-draw/bending test [26] was used to quantitatively investigate the effect of Bauschinger effect and transient behavior, permanent softening and unloading modulus on springback prediction. Although the analysis of real parts would be practical for industrial applications, it is difficult to differentiate the error sources of the inaccuracy of springback prediction with such complicated geometries. Thus it is better to fix the other aspects of error sources such as anisotropy, contact, element type, while focus on the influence of hardening behavior on springback prediction. The following subsections summarize the descriptions of U-draw/bending test, its finite element model and the material parameters as well.

3.1. Description

The first version of U-draw/bending springback problem was presented in Numisheet'93 benchmark. Since the material in sidewall mainly experiences bending, unloading, reverse bending, and unloading, this benchmark is very suitable to evaluate the capability of hardening model in the modelling of the mechanical behavior under reverse loading. So far, many hardening models have been evaluated by means of numerical simulation [9,35] and analytical method [36] using this U-draw/bending test. With the increasing applications of advanced high strength steels (AHSSs) in automotive industries, multi-step forming processes might be required due to the poor ductility of AHSS [26]. Then it would be important to understand how the pre-strain caused by current forming influences on subsequent forming and final springback. Therefore, the U-draw/bending test in Numisheet'93 benchmark was recently updated with as-received and pre-strained sheets as a Numisheet2011 benchmark problem [26].

The geometry and dimensions of the U-draw/bending test in Numisheet2011 benchmark report [26] are illustrated in Fig. 2. The material near the punch corner dominantly experiences bending and unloading. In such a situation, the predicted springback θ_1 (see Fig. 3) is mainly determined by the stress response under monotonic loading and unloading modulus. It is not related to the modeling of Bauschinger effect and transient behavior. As for the materials in sidewall, they underwent one cyclic loading as already mentioned. Then the predicted springback is not only determined by the reverse unloading behavior but also significantly influenced by the strain range before reverse unloading. This is because the stress response under reverse loading at different strain ranges might involve the contributions of Bauschinger effect, transient behavior and/or permanent softening. Thus the springback parameters θ_2 and ρ are defined to quantitatively evaluate the springback behavior of the materials in sidewall (see Fig. 3).

For the material, a dual phase steel DP780 with 1.4 mm thickness was considered. Two kinds of specimens are used for U-draw/bending: one with as-received material (without pre-strain) and the other with pre-stretching by 8% in engineering strain along rolling direction. Rectangular shaped specimens are used for both cases. Their dimensions are 360.0 mm in length and 30.0 mm in width. For the pre-strain case, the specimens with the length of 360.0 mm were griped to perform the uni-axial tensile tests along rolling direction. The length of grip end is 25.0 mm for both sides. And then, the specimen for subsequent U-draw/bending test was cut out from the central portion of the pre-stretched specimen. Finally, the length of the specimen was 324.0 mm after 8% pre-stretching and subsequent trimming [26]. Blank holding force of 2.94 kN was maintained by the blank holder (see Fig. 2) during the U-draw/bending procedure. For lubrication, P-340N was applied on the tool surfaces and the blank. The punch speed was 1.0 mm/s and the stroke was 71.8 mm after initial contact between the punch and the blank.

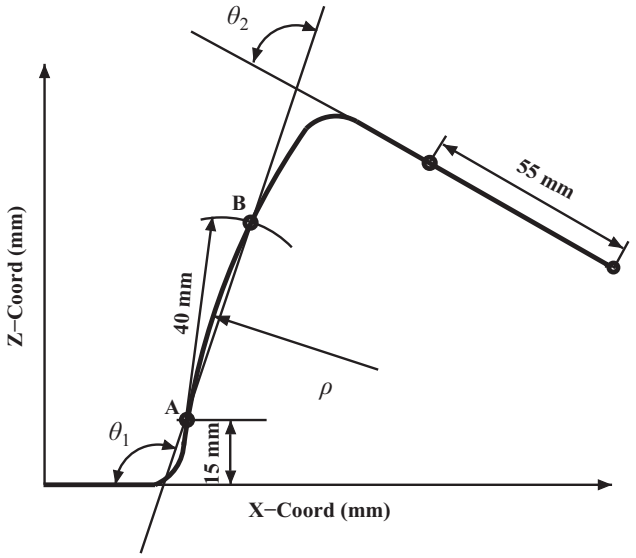

Fig. 3. Definition of the springback.

3.2. Finite element model

The finite element models for U-draw/bending test were constructed in Abaqus version 6.10 [11]. Five analysis steps are involved in the numerical simulations of the pre-strained U-draw/bending test, which are (i) pre-stretching along rolling direction, (ii) unloading, (iii) applying the blank holder force, (iv) U-draw/bending procedure and (v) springback. The first two analysis steps were first simulated in the implicit code Abaqus/Standard. Then, the deformed state was imported into the explicit code Abaqus/Explicit to form the U-shaped part, and finally the state after forming was again imported into the implicit code Abaqus/Standard to get the final unloading part. As for the pre-strain case, the specimen with a length of 310.0 mm was stretched to the engineering strain of 8% in the numerical simulation. It means that the length of deformed specimen is 334.8 mm before unloading. After unloading procedure, the specimen was used in the numerical simulation of U-draw/bending springback problem. Comparing with the length of experimental trimmed specimen (324.0 mm), the impact resulted from the present simplicity was believed to be slight. To accurately describe the anisotropic behavior of metallic sheets, the non-quadratic anisotropic yield function Yld2000-2d was chosen due to its good accuracy [6]. Also, note that the resulting constitutive model can be associated with any anisotropic yield function. For the hardening behavior, the Bauschinger effect, transient behavior and permanent softening were captured by the ANK model. The ANK model incorporating a

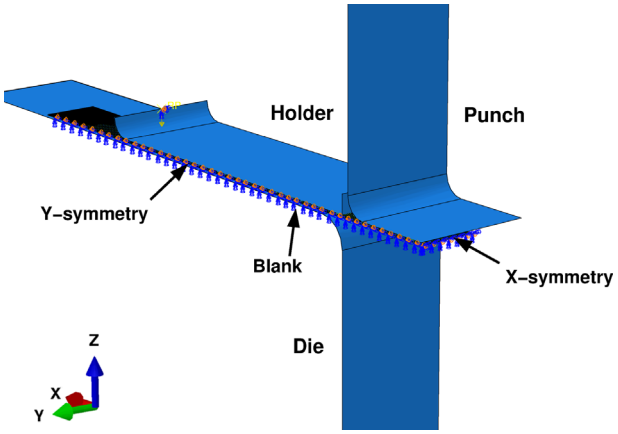

Fig. 4. Initial set-up of the U-draw/bending for finite element simulation.

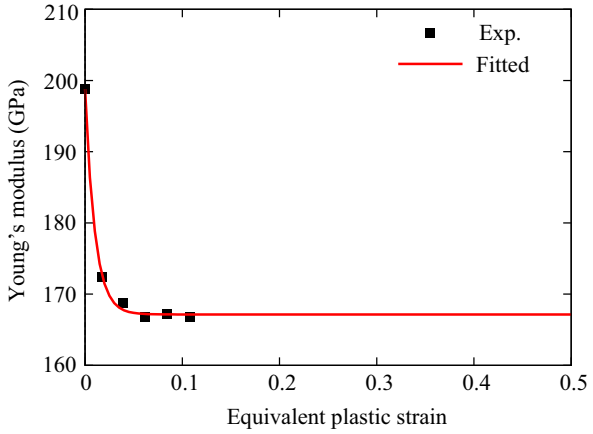

Fig. 5. Young's modulus vs. equivalent plastic strain in the uniaxial tension state.

Table 1
Coefficients of Yld2000-2d anisotropic yield function.

Material	Parameters	Values
DP780	α_1	0.9276
	α_2	1.0243
	α_3	0.9622
	α_4	0.9980
	α_5	1.0043
	α_6	0.9165
	α_7	1.0043
	α_8	1.0324
	m	6.0

Table 2
Material parameters of the hardening models for DP780.

Parameter	Unit	ANK model
$\sigma_\circ$	MPa	527.0
C_1	MPa	10154.2
γ_1	–	44.1
C_2	MPa	124.2
Q	MPa	402.0
b	–	29.9

changed unloading modulus as a function of plastic strain was implemented into Abaqus package through the material user subroutines UMAT (Abaqus/Standard) and VUMAT (Abaqus/Explicit). Considering the symmetry of the model and boundary condition, a quarter of the rectangular blank was simulated. As shown in Fig. 4, a three dimensional finite element model was used. The analytical rigid-body element was chosen for tools (punch, die and blank holder). The reduced 4-node shell element (S4R) was employed for the blank. A mesh size of 0.5 mm $\times$ 0.75 mm (length $\times$ width) and 9 Simpson integration points through the thickness were chosen. The Coulomb friction coefficient between tools and the blank was 0.1, as recommended by the Numisheet2011 benchmark report [26].

3.3. Material parameters

The material parameters of the current constitutive model can be categorized into three aspects, coefficients of Yld2000-2d anisotropic yield function, hardening parameters and the parameters related to the change of unloading modulus. Regarding the coefficients of Yld2000-2d anisotropic yield function (see Appendix A), they were provided in the benchmark report [26], as listed in Table 1.

For the effect of pre-strain on unloading modulus, [15] and [37] concluded that unloading modulus can be expressed as a scalar function of equivalent plastic strain in view of the experimental observations on stress vs. strain curves of uni-axial and bi-axial cyclic loadings. To describe such a pre-strain dependency of unloading modulus, a saturated type function of equivalent plastic strain was proposed by [15], and have been widely used [20,21,38]. Usually, the unloading modulus is formulated as

$$E = E_0 - (E_0 - E_a)[1 - e^{(-\xi\bar{\varepsilon}^p)}] \tag{24}$$

where E_a and ξ are two material parameters, E_0 is the initial elastic modulus. In the benchmark report of Numisheet2011 [26], the experimental unloading modulus with respect to the pre-strain during the reverse loading state has been provided for DP780 steel. The initial value of Young's modulus of DP780 steel is 198.8 GPa. By fitting these experimental unloading modulus with Eq. (24), E_a and ξ were determined to be 167.15 GPa and 99.55, respectively. As shown in Fig. 5, the unloading modulus rapidly decreases and saturates to E_a as the equivalent plastic strain increases. Since the critical equivalent plastic strain is very small, around 0.02, it can be inferred that the effect of pre-strain on elastic modulus might be approximated as the saturated constant value, E_a.

As for the hardening parameters, an inverse identification was carried out using uni-axial tension, tension-compression-tension (TCT) with an in-house Matlab toolbox SMAT. The true stress vs. strain curves of uni-axial tension along three different loading directions, i.e., 0°, 45° and 90° from the rolling direction (RD), were provided in the Numisheet2011 benchmark report [26]. In addition, the in-plane TCT tests were also performed for the measurement of the true stress vs. strain curves under cyclic loading in the benchmark. Five different pre-strains are available for the TCT tests, which are approximately 2%, 4%, 6%, 8% and 10%. With these experimental data, the hardening parameters in the ANK model, $\sigma_\circ$, C_1, γ_1, C_2, Q and b, are optimized at the same time. In the Matlab toolbox SMAT, a cost function $\mathcal{L}(\boldsymbol{A})$ was defined in the least square sense by Eq. (25) with an initial guess of hardening parameters $\boldsymbol{A}_0$. The cost function is minimized with a Levenberg–Marquardt algorithm.

$$\mathcal{L}(\boldsymbol{A}) = \sum_{n=1}^{N} \mathcal{L}_n(\boldsymbol{A}) = \sum \mathcal{L}_n^{T-S}(\boldsymbol{A}) + \sum_{\beta} \mathcal{L}_n^{TCT-S}(\boldsymbol{A}) \tag{25}$$

where N is the number of tests in the database. Superscript 'T-S' stands for the stress level in uni-axial tension. 'TCT-S' stands for

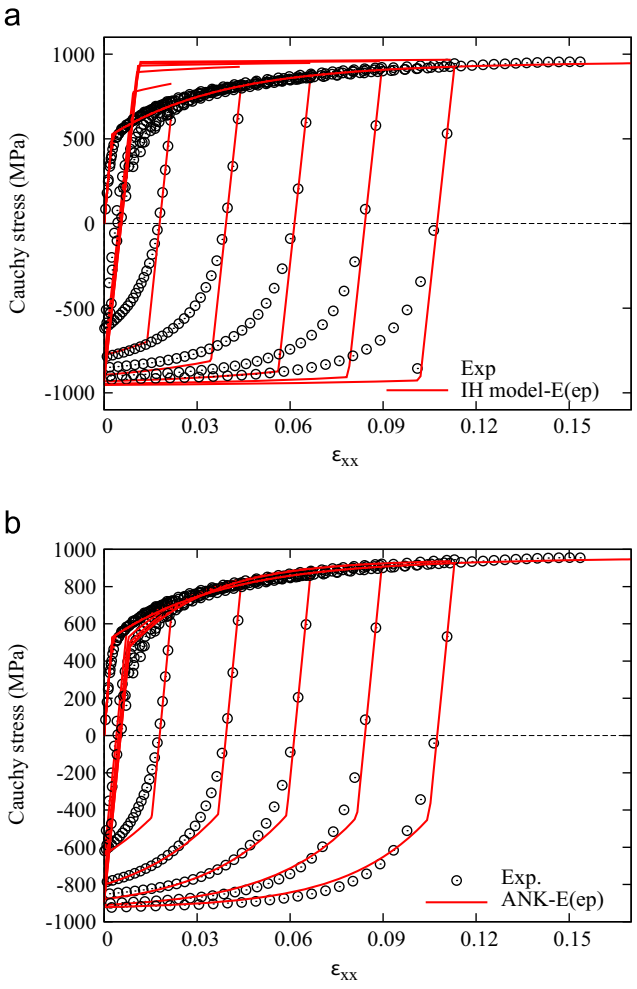

Fig. 6. Predicted tension–compression–tension true stress vs. strain curves, where the Young's modulus variation is considered. (a) Isotropic hardening model and (b) The ANK model.

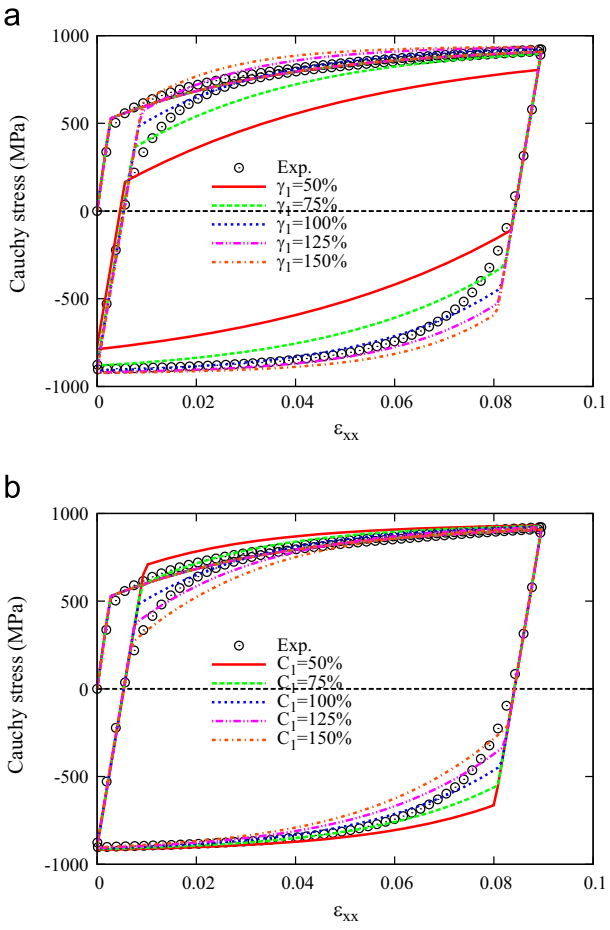

Fig. 7. Predicted stress–strain curves with different Bauschinger effect and transient behavior. (a) Impact of γ_1 on predicted stress–strain curves, C_1 is fixed and (b) Impact of C_1/γ_1 on predicted stress–strain curves, γ_1 is fixed.

the stress level in tension-compression-tension. The sum β for tension-compression-tension is performed over all pre-strains. For each test, the gap between experiments and model is given by

$$\mathcal{L}_n(\boldsymbol{A}) = \frac{1}{M_n}\sum_{i=1}^{M_n}(\boldsymbol{Z}(\boldsymbol{A},t_i)-\boldsymbol{Z}^*(t_i))^T\mathcal{D}_n(\boldsymbol{Z}(\boldsymbol{A},t_i)-\boldsymbol{Z}^*(t_i)) \tag{26}$$

where M_n is the number of experimental points of the n-th test, $\boldsymbol{Z}(\boldsymbol{A},t_i)-\boldsymbol{Z}^*(t_i)$ is the gap between experimental $\boldsymbol{Z}^*$ and simulated output variables $\boldsymbol{Z}$ at time t_i, and $\mathcal{D}_n$ is a weighting matrix for the n-th test. Finally, the optimized hardening parameters are shown in Table 2. The predicted true stress response with these parameters are also plotted in Fig. 6.

Additionally, it is worth noting that a special isotropic hardening law was adopted in Fig. 6(a), which can be written as

$$\sigma^{\circ} = \sigma_{\circ} + R_{iso} = \sigma_{\circ} + Q(1-e^{-b\bar{\varepsilon}^p}) + C_2\bar{\varepsilon}^p \tag{27}$$

where the parameters $\sigma_{\circ}$, Q, b and C_2 are the same as those of the ANK model. Comparing Eqs. (18) and (27), it is obvious that the predicted flow stresses will be absolutely the same as uni-axial tension. As already mentioned, this is very important to quantitatively estimate the significance of the Bauschinger effect, transient behavior and permanent softening in evaluating their influences on springback simulation. The details will be further discussed in Section 4.2.

4. Results and discussion

Since the present works focus on studying the influences of the hardening and unloading behavior under strain reversal on springback prediction, the effect of initial anisotropy should be excluded. Samples used in the current U-draw/bending springback problem are all aligned along the rolling direction, which is same as the reference direction of flow stress in the constitutive model. In addition, the strips are narrow that the deformation of materials is almost uni-axial tension. Moreover, the anisotropy of DP780 steel is quite small [38]. Therefore, it can be inferred that the influence of initial anisotropy on predicted springback in the present work has been minimized. It also indicates that the simulated springback from anisotropic yield function Yld2000-2d and isotropic yield function von Mises would be almost same.

4.1. Sensitivity analysis for the effect of Bauschinger effect and unloading modulus on springback

To investigate the effect of the Bauschinger effect and transient behavior on springback, a sensitivity analysis was conducted here. For efficient sensitivity analysis, the simulated flow stress during forward tension, and permanent softening under reversed loading should be exactly same when the material parameters related to the Bauschinger effect and transient behavior are varied. For the ANK model [25], material parameters C_1 and γ_1 are related to the Bauschinger effect and transient behavior. Meanwhile, the hardening parameters, $\sigma_{\circ}$, Q, b and C_2, only influence the isotropic

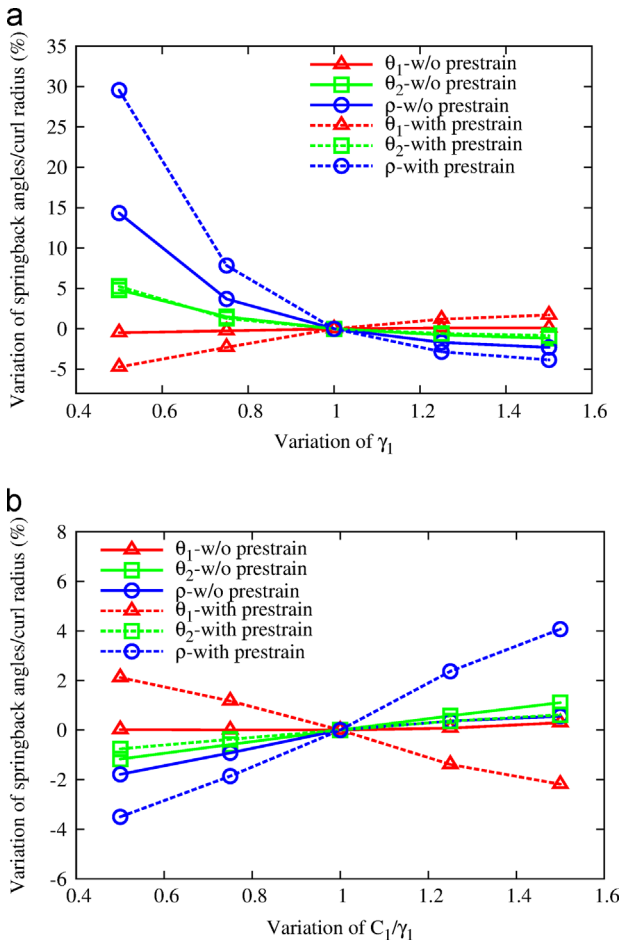

Fig. 8. Sensitivity analysis of the Bauschinger effect and transient behavior on predicted springback parameters. (a) Impact of γ_1 on predicted springback parameters, C_1 is fixed and (b) Impact of C_1/γ_1 on predicted springback parameters, γ_1 is fixed.

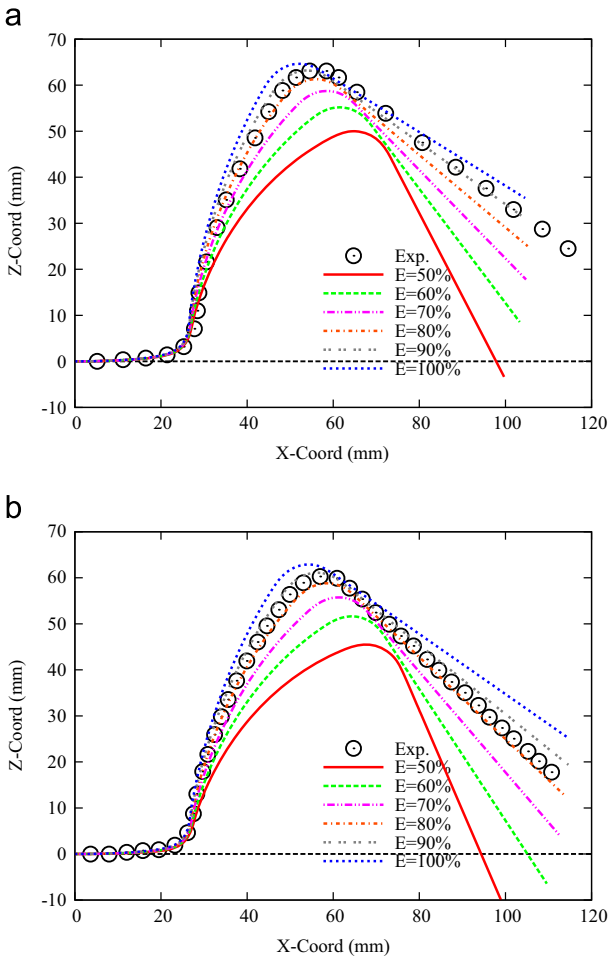

Fig. 9. Influences of the Young's modulus on predicted springback profile. (a) Blank without pre-strain and (b) Blank with pre-strain.

hardening and permanent softening as indicated by Eqs. (16) and (22). Therefore, the variation of simulated Bauschinger effect and transient behavior can be easily obtained by the parameters C_1 or γ_1. In the present work, the hardening parameters listed in Table 2 are considered as the reference set.

Fig. 7 shows the effect of C_1 and γ_1 on the Bauschinger effect and transient behavior for the uniaxial tension-compression-tension. It is shown in Fig. 7(a) that the flow stress under strain reversal increases as γ_1 increases, but eventually saturates. This is because γ_1 only determines the hardening rate of the backstress in the kinematic hardening model. Smaller γ_1 needs more plastic deformation to saturate toward C_1/γ_1. Similarly, the influence of C_1 on the simulated flow stress is also investigated as shown in Fig. 7(b). The results show that the yield stress at reversed curves decreases as C_1 increases. However, the plastic deformation leading to the saturated reversed stress is not correlated to the variation of parameters C_1. Moreover, Eq. (22) states that either smaller C_1 or larger γ_1 will lead to faster convergence of $\Delta\sigma$ to a certain constant value. Consequently, the simulated flow stresses under strain reversal will result in similar saturated values either when γ_1 is very large, or when C_1 is very small.

Fig. 8 shows the influences of C_1 and γ_1 on predicted springback parameters. For the effect of γ_1, Fig. 8(a) shows that the variations of springback increases as γ_1 decreases. But the variations on predicted springback tend to decreases as γ_1 increases. This is because the stress vs. strain curves are not much different when γ_1 is large enough as shown in Fig. 7(a). Fig. 8(b) shows that almost linear relationship is resulted in between C_1 and variations of springback. Comparing with the effect of γ_1, C_1 has less effect on the amount of predicted springback. For both parameters C_1 and γ_1, the variations of sidewall curl (ρ) are noticeable. It means that the hardening behavior under strain reversal has more significant influence on the springback since the material at sidewall mainly experiences loading–unloading–reverse loading. However, the hardening behavior under reverse loading involves the Bauschinger effect, transient behavior and permanent softening as illustrated in Fig. 1. It seems difficult to conclude which behavior plays more important role by only considering the effects of γ_1 and C_1. Therefore, a quantitative comparison will be further discussed in the next Section 4.2.

Additionally, the effect of apparent elastic modulus at unloading was also investigated by conducting the simulations with constant initial modulus E_0 and saturated modulus E_a after prestrain. Here, E_a values are used as fractions of the initial Young's modulus; i.e., 100%, 90%, 80%, 70%, 60% and 50% of E_0 are chosen. Fig. 9 shows the influences of unloading modulus on the simulated springback. The ANK model was used for pre-strained blank. It is found that the springback gradually increases as the saturated unloading modulus decreases. Although there is a rapid decrease at the beginning of the variable modulus as shown in Fig. 5, the unloading modulus almost saturates to the reference set E_a for the case of pre-strained blank. Therefore, this rapid decrease of unloading modulus has no influence on predicted springback.

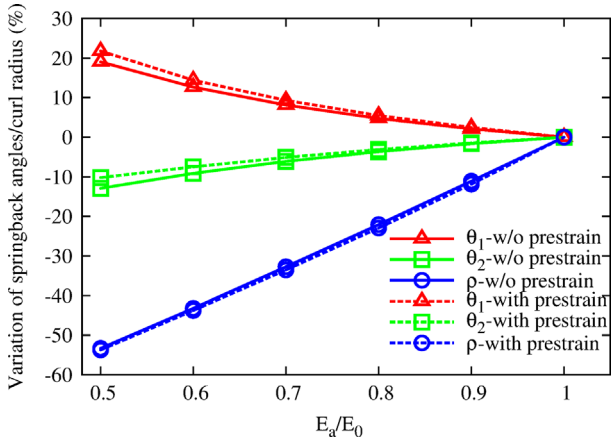

Fig. 10. Sensitivity analysis of the Young's modulus on predicted springback parameters.

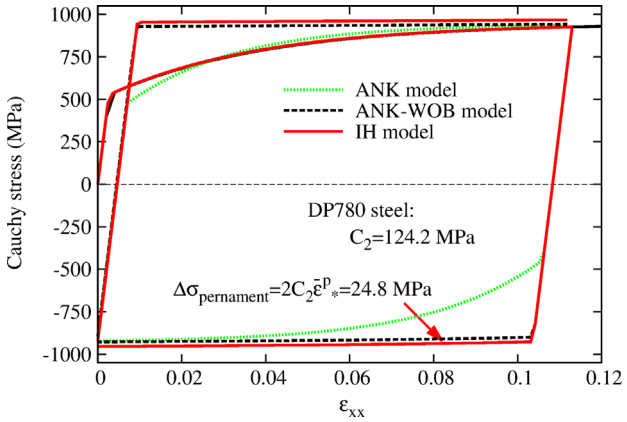

Fig. 11. Predicted stress–strain curves with different hardening models.

From Fig. 9, it is found that the sheet with pre-strain seems to represent larger springback than the case without pre-strain when the saturated unloading modulus E_a decreases. In addition, the springback parameters are normalized relative to the case of $E_a = E_0$, as shown in Fig. 10. The results show that the influence of unloading modulus on predicted springback is almost linear. With the decrease of unloading modulus, the variations of predicted springback tend to be large. It is easy to understand that a larger springback will be predicted by a smaller unloading modulus since the springback recovery is inversely proportional to unloading modulus.

4.2. Estimating the significance of each hardening behavior and unloading modulus

In the previous subsection, the sensitivity analysis implies that both hardening behavior under reverse loading and unloading modulus have significant effects on springback prediction. In this subsection, the contributions of the Bauschinger effect and transient behavior, permanent softening, and unloading modulus to the final predicted springback will be estimated using the special feature of the ANK model [25]. In other words, individual contribution from each hardening behavior will be estimated.

As already known, the magnitude of springback is proportional to the stress level before unloading and inversely proportional to unloading modulus. To quantitatively estimate the influences of Bauschinger effect and transient behavior, permanent softening and changes of unloading modulus, the variable U is introduced to

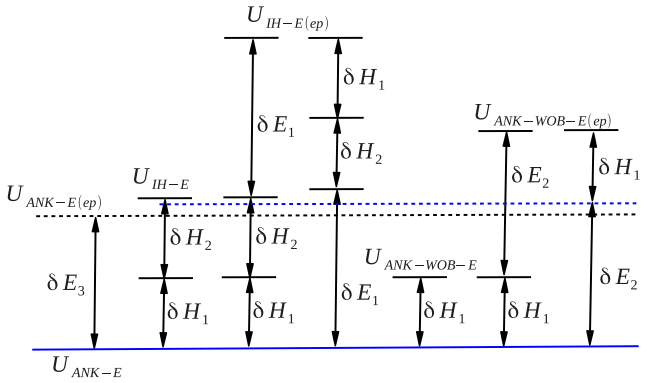

Fig. 12. A schematic illustration of the influences of hardening and unloading behavior on simulated springback.

represent the amount of U-draw/bending springback, which is one of the parameters θ_1, θ_2 and ρ.

Without loss of generality, the classical isotropic hardening (namely IH) and the ANK models with/without Bauschinger effect and transient behavior (namely ANK/ANK-WOB) are respectively considered for hardening models. Here, the ANK model without the Bauschinger effect and transient behavior (ANK-WOB) plays an important role for this estimation. The ANK-WOB model means that the Bauschinger effect and transient behavior described by Eq. (8a) are neglected. It is achieved by modifying the parameter γ_1 to a very large value (5000 was used in this study) in the ANK model [25]. As already explained, a large γ_1 will lead the backstress rapidly saturate to the constant value. Then, the effect of Bauschinger effect and transient behavior during strain reversal will be minimized. Fig. 11 shows that isotropic hardening model always overestimates the flow stress by the ANK-WOB model by a constant offset stress. It is also shown that the stress simulated by the ANK model under strain reversal saturates to that of the ANK-WOB model after a large plastic deformation. Moreover, the change of unloading modulus is considered as well, $E(ep)$ denotes the unloading modulus as a function of plastic deformation, while E is an initial Young's modulus.

For conveniences, the following definitions are introduced here,

$$\delta_{H1} = U_{ANK-WOB-E} - U_{ANK-E} \tag{28a}$$

$$\delta_{H2} = U_{IH-E} - U_{ANK-WOB-E} \tag{28b}$$

$$\delta_{E1} = U_{IH-E(ep)} - U_{IH-E} \tag{28c}$$

$$\delta_{E2} = U_{ANK-WOB-E(ep)} - U_{ANK-WOB-E} \tag{28d}$$

$$\delta_{E3} = U_{ANK-E(ep)} - U_{ANK-E} \tag{28e}$$

Since the difference between the ANK-WOB and ANK models is the existence of the Bauschinger effect and transient behavior in the predicted stress–strain curves, the gap δH_1 can be used to represent the effect of the Bauschinger effect and transient behavior on predicted springback. Similarly, δH_2 stands for the influence of permanent softening on springback prediction. Regarding the effect of unloading modulus, it can be respectively described by the parameters δE_1, δE_2 and δE_3.

Since the ANK model is able to describe the realistic stress–strain curves of sheet metals, we assumed that the ANK model with an unloading modulus as a function of plastic deformation has the highest accuracy in springback prediction. Then, the simulated springback from the other models can be rewritten as

$$U_{IH-E} = U_{ANK-E(ep)} - \delta_{E3} + \delta_{H2} + \delta_{H1} \tag{29a}$$

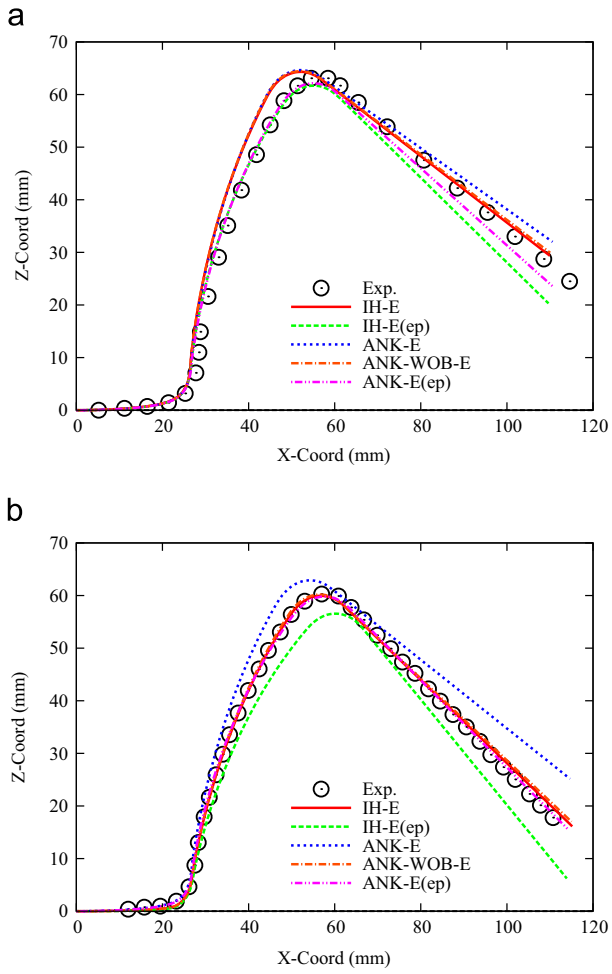

Fig. 13. Experimental and predicted springback profiles after U-draw/bending. (a) Blank without pre-strain and (b) Blank with pre-strain.

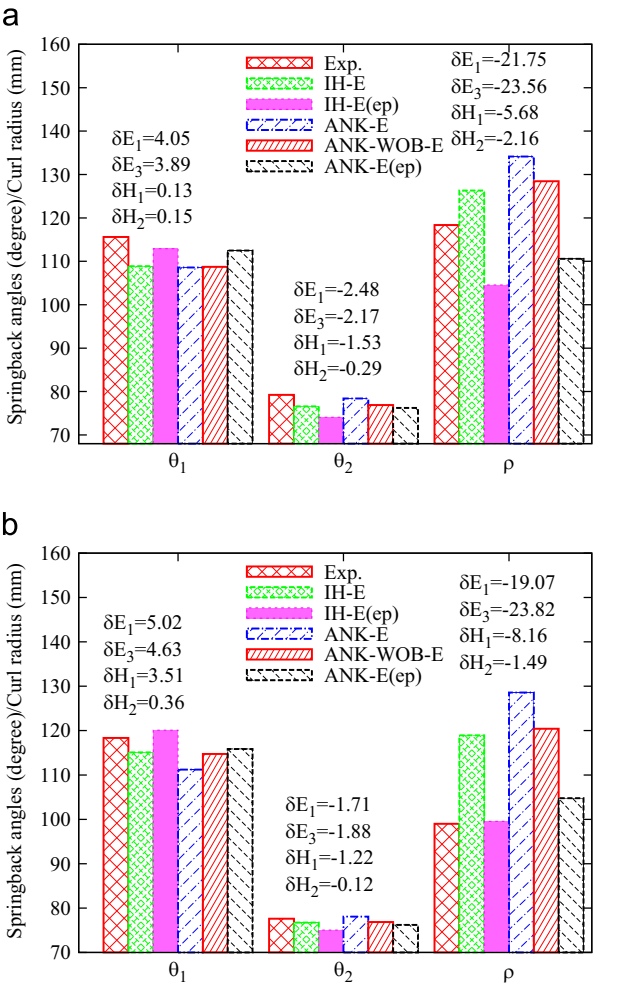

Fig. 14. Experimental and predicted springback parameters after U-draw/bending. (a) Blank without pre-strain and (b) Blank with pre-strain.

$$U_{IH-E(ep)} = U_{ANK-E(ep)} - \delta_{E3} + \delta_{H2} + \delta_{H1} + \delta_{E1} \tag{29b}$$

$$U_{ANK-WOB-E} = U_{ANK-E(ep)} - \delta_{E3} + \delta_{H1} \tag{29c}$$

$$U_{ANK-WOB-E(ep)} = U_{ANK-E(ep)} - \delta_{E3} + \delta_{H1} + \delta_{E2} \tag{29d}$$

$$U_{ANK-E} = U_{ANK-E(ep)} - \delta_{E3} \tag{29d}$$

The qualitative comparisons for the predicted springback in Eqs. (29) are illustrated in Fig. 12. It can be inferred that the springback predicted from the ANK model with changed unloading modulus, i.e., $U_{ANK-E(ep)}$, locates between the amount of springback U_{ANK-E} and $U_{ANK-E}+\delta E_2$ all the time. This is due to the fact that the magnitude of δ_{E3} is less than those of δ_{E1} and δ_{E2} all the time. However, for the predicted springback U_{IH-E} and $U_{ANK-WOB-E}$, their relative relationships to $U_{ANK-E(ep)}$ are unknown because the relative relation between δE_3 and $\delta H_1/\delta H_2$ depends on the material itself. Therefore, there is a possibility that the springback predicted by the isotropic hardening with initial Young's modulus is close to the real springback. This can be explained easily if we assume that $U_{ANK-E(ep)}$ is real solution which is exactly the same as the experiment. Then, isotropic hardening assumption always overestimates the springback, which makes the predicted springback away from experiment. But, initial elastic modulus assumption decreases the springback, which leads to the prediction closer to experiment. Overall, the isotropic hardening with initial elastic modulus sometimes results in good match with experiment. However, it is worth noting that this possibility does not indicate that the advanced constitutive models are not necessary in sheet springback prediction.

Fig. 13 shows the experimental and predicted springback profiles after U-draw/bending for different models. It is found that the ANK model [25] with a changed unloading modulus represents the best agreement with experiments. The hardening models with changed unloading modulus always predict larger springback compared with those with an initial unloading modulus. In the case of constant initial unloading modulus, isotropic hardening predicts slight larger springback than that of the ANK-WOB model. Since the permanent softening for the DP780 steel is not significant (see Fig. 11), this small difference between the springback amount predicted by isotropic hardening and the ANK-WOB model is reasonable. A large gap is observed for the springback predicted by the ANK model (ANK-E(ep)) and isotropic hardening (IH-E(ep)). It indicates that the Bauschinger effect and transient behavior might play an important role in the springback prediction. It is worth noting that the springback predicted by isotropic hardening model with a constant initial unloading modulus is very close to the experimental results for the pre-strained blank. On the other hand, there is an obvious difference in sidewall profile prediction in case of blank without pre-strain. As already mentioned, there is a possibility for the isotropic hardening model with a constant initial unloading modulus to predict the springback close to the actual amount. But it should be emphasized that the error considerably depends on the material and its deformation history. Logically, there is no consistent springback

predictions for isotropic hardening model with a constant initial unloading modulus.

To quantitatively compare the contributions of the Bauschinger effect and transient behavior, permanent softening and unloading modulus to the predicted springback, δE_1, δE_2, δH_1 and δH_2 are respectively calculated for the springback parameters θ_1, θ_2 and ρ (see Fig. 14). For the DP780 steel, it can be seen that the variation of predicted springback resulted from the decrease of unloading modulus is much larger than those from the Bauschinger effect and permanent softening; i.e., δE_1 or δE_3 is larger than the sum of δH_1 and δH_2. This is because the flow stress of DP780 steel is higher and it is known that the unloading modulus seems more important for such high strength steels [20]. Since the permanent softening is small for DP780 steel as shown in Fig. 11, the influence of Bauschinger effect and transient behavior on predicted springback is more serious than that of permanent softening for sidewall prediction (ρ). Moreover, it is found that the Bauschinger effect and transient behavior seem to be important for the springback parameter θ_1 in the case with pre-strain. In such a case, the material near the punch corner, which corresponds to the springback parameter θ_1, experience continuous tension (bottom surface) and pre-strained tension-compression (top surface). Since there is a strain path change for the material at the top surface of blank, the Bauschinger effect, transient behavior and permanent softening should have significant effect on the predicted springback.

Although the Bauschinger effect, transient behavior, permanent softening and unloading modulus for different kinds of material are not exact same, we still can get some general descriptions on the same kind of material. For instance, the change of unloading modulus for dual phase steels is similar, and the permanent softening is usually slight [16,20]. Therefore, for the same kind of material, if we adopted the present method to estimate the significance of each hardening behavior and unloading modulus, the derived conclusions are meaningful in some senses.

5. Conclusion

In the present work, the influences of the Bauschinger effect and transient behavior, permanent softening and unloading behavior of metallic sheets on springback prediction were quantitatively estimated using the special feature of the ANK model. Three different hardening schemes were considered by properly selecting material parameters of the ANK model: isotropic hardening (IH); isotropic-kinematic hardening with Bauschinger effect and transient behavior, and permanent softening (ANK model); isotropic-kinematic hardening with only permanent softening (ANK-WOB model). During monotonic loading, all these models produce exactly the same uni-axial plastic flow stress curves. Under strain reversal, ANK-WOB model only considers permanent softening, while ANK model takes into account the Bauschinger effect and transient behavior, as well as permanent softening. Moreover, the degradation of elastic modulus after plastic pre-strain was also considered for each hardening model. The springback problem of U-draw/bending of as-received and pre-strained DP780 steel was predicted by these three hardening models with/without the change of unloading modulus. For DP780 steel considered in this study, the results showed that the unloading modulus is more important than the Bauschinger effect and transient behavior, and permanent softening in springback prediction. Meanwhile, the Bauschinger effect and transient behavior are highly influential for springback prediction comparing with permanent softening. In addition, the relative relationships among the springback predicted by different hardening models with/without the change of unloading modulus are qualitatively compared. Through the detailed parametric study for the effect of hardening and elastic unloading behavior, the conventionally adopted isotropic hardening scheme with constant initial elastic modulus might be able to predict the springback within reasonable accuracy, but the analysis showed that this does not justify the appropriateness of the model.

Acknowledgments

Shun-lai Zang would like acknowledge financial support by the National Natural Science Foundation of China (no.11002105) and by the Opening Project of Key Laboratory of Testing Technology for Manufacturing Process (Southwest University of Science and Technology), Ministry of Education (no.10ZXZK03). Myoung-gyu Lee appreciates the partial support by the grants from the ERC program of NRF of Korea and from the basic science and research program (2011-009801).

Appendix A. Anisotropic yield function Yld2000-2d

The non-quadratic anisotropic yield function Yld2000-2d is a linear transformation of two convex functions ϕ' and ϕ'' [6]. It is defined by an equivalent stress $\overline{\sigma}$:

$$\phi(\boldsymbol{s}) = \overline{\sigma} = \left[\frac{1}{2}(\phi' + \phi'')\right]^{\frac{1}{m}} \tag{A.1}$$

where

$$\phi' = |S_1' - S_2'|^m; \quad \phi'' = |2S_2'' + S_1''|^m + |2S_1'' + S_2''|^m \tag{A.2}$$

with $m=6$ and $m=8$ for BCC and FCC materials, respectively. $S_{1,2}'$ and $S_{1,2}''$ are the principal values of the linear transformations on the stress deviator $\tilde{\boldsymbol{s}}'$ and $\tilde{\boldsymbol{s}}''$ which are defined as

$$\begin{bmatrix} \tilde{s}_{11}' \\ \tilde{s}_{22}' \\ \tilde{s}_{12}' \end{bmatrix} = \begin{bmatrix} C_{11}' & C_{12}' & 0 \\ C_{21}' & C_{22}' & 0 \\ 0 & 0 & C_{44}' \end{bmatrix} \begin{bmatrix} s_{11} \\ s_{22} \\ s_{12} \end{bmatrix} \tag{A.3}$$

and

$$\begin{bmatrix} \tilde{s}_{11}'' \\ \tilde{s}_{22}'' \\ \tilde{s}_{12}'' \end{bmatrix} = \begin{bmatrix} C''_{11} & C_{12}'' & 0 \\ C''_{21} & C_{22}'' & 0 \\ 0 & 0 & C_{44}'' \end{bmatrix} \begin{bmatrix} s_{11} \\ s_{22} \\ s_{12} \end{bmatrix} \tag{A.4}$$

where $\boldsymbol{C}'$ and $\boldsymbol{C}''$ are linear transformation matrices. s_{11}, s_{22} and s_{12} are the components of the deviatoric stress tensor $\boldsymbol{s}$.

Using

$$\boldsymbol{T} = \begin{bmatrix} 2/3 & -1/3 & 0 \\ -1/3 & 2/3 & 0 \\ 0 & 0 & 1 \end{bmatrix} \tag{A.5}$$

the transformation can be applied on the Cauchy stress tensor $\boldsymbol{\sigma}^T = (\sigma_{11}, \sigma_{22}, \sigma_{12})$ as

$$\tilde{\boldsymbol{s}}' = \boldsymbol{C}' \cdot \boldsymbol{s} = \boldsymbol{C}' \cdot \boldsymbol{T}\boldsymbol{\sigma} = \boldsymbol{L}' \cdot \boldsymbol{\sigma} \tag{A.6}$$

and

$$\tilde{\boldsymbol{s}}'' = \boldsymbol{C}'' \cdot \boldsymbol{s} = \boldsymbol{C}'' \cdot \boldsymbol{T}\boldsymbol{\sigma} = \boldsymbol{L}'' \cdot \boldsymbol{\sigma} \tag{A.7}$$

The tensors $\boldsymbol{L}'$ and $\boldsymbol{L}''$ representing linear transformation of the stress tensor are

$$\begin{bmatrix} L_{11}' \\ L_{12}' \\ L_{21}' \\ L_{22}' \\ L_{66}' \end{bmatrix} = \begin{bmatrix} 2/3 & 0 & 0 \\ -1/3 & 0 & 0 \\ 0 & -1/3 & 0 \\ 0 & 2/3 & 0 \\ 0 & 0 & 1 \end{bmatrix} \begin{bmatrix} \alpha_1 \\ \alpha_2 \\ \alpha_7 \end{bmatrix} \tag{A.8}$$

and

$$\begin{bmatrix} L''_{11} \\ L''_{12} \\ L''_{21} \\ L''_{22} \\ L''_{66} \end{bmatrix} = \frac{1}{9} \begin{bmatrix} -2 & 2 & 8 & -2 & 0 \\ 1 & -4 & -4 & 4 & 0 \\ 4 & -4 & -4 & 1 & 0 \\ -2 & 8 & 2 & -2 & 0 \\ 0 & 0 & 0 & 0 & 9 \end{bmatrix} \begin{bmatrix} \alpha_3 \\ \alpha_4 \\ \alpha_5 \\ \alpha_6 \\ \alpha_8 \end{bmatrix} \tag{A.9}$$

where all the independent coefficients α_k (for $k: 1-8$) reduce to 1 in isotropic case. For the calibration of material coefficients α_k, only seven coefficients are required to account for seven input data, namely σ_0, σ_{45}, σ_{90}, r_0, r_{45}, r_{90}, the uni-axial yield stresses and r-values measured at 0°, 45°, 90° to RD, and σ_b the balanced bi-axial yield stress. The eighth input data can be the ratio $r_b = \dot{\varepsilon}^p_{22}/\dot{\varepsilon}^p_{11}$, which characterizes the slope of the yield surface in balanced bi-axial tension.

References

[1] Lee M-G, Kim D, Kim C, Wenner ML, Chung K. Spring-back evaluation of automotive sheets based on isotropic-kinematic hardening laws and non-quadratic anisotropic yield functions, part iii: applications. Int J Plast 2005;21:915–53.

[2] Yoshida F, Uemori T. A model of large-strain cyclic plasticity and its application to springback simulation. Int J Mech Sci 2003;45:1687–702.

[3] Li K, Carden W, Wagoner R. Simulation of springback. Int J Mech Sci 2002;44:103–22.

[4] Wagoner R, Li M. Simulation of springback: through-thickness integration. Int J Plast 2007;23:345–60.

[5] Barlat F, Lian K. Plastic behavior and stretchability of sheet metals. Part i: a yield function for orthotropic sheets under plane stress conditions. Int J Plast 1989;5:51–66.

[6] Barlat F, Brem J, Yoon J, Chung K, Dick R, Lege D, et al. Plane stress yield function for aluminum alloy sheets. Part 1: theory. Int J Plast 2003;19:1297–319.

[7] Barlat F, Gracio JJ, Lee M-G, Rauch EF, Vincze G. An alternative to kinematic hardening in classical plasticity. Int J Plast 2011;27:1309–27.

[8] Karafillis A, Boyce M. A general anisotropic yield criterion using bounds and a transformation weighting tensor. J Mech Phys Solids 1993;41:1859–86.

[9] Lee M-G, Kim D, Kim C, Wenner M, Wagoner R, Chung K. A practical two-surface plasticity model and its application to spring-back prediction. Int J Plast 2007;23:1189–212.

[10] Zhu Y, Liu Y, Yang H, Li H. Development and application of the material constitutive model in springback prediction of cold-bending. Mater Des 2012;42:245–58.

[11] ABAQUS, User's manual (version 6.10). Hibbit, Karlsson & Sorensen Inc. USA.; 2010.

[12] LSTC, LS-DYNA users manual (version 971). Livermore Software Technology Corporation, CA, USA, 2006.

[13] Boger R, Wagoner R, Barlat F, Lee M, Chung K. Continuous, large strain, tension/compression testing of sheet material. Int J Plast 2005;21:2319–43.

[14] Bouvier S, Haddadi H, Leve P, Teodosiu C. Simple shear tests: experimental techniques and characterization of the plastic anisotropy of rolled sheets at large strains. J Mater Process Technol 2006;172:96–103.

[15] Yoshida F, Uemori T, Fujiwara K. Elastic-plastic behavior of steel sheets under in-plane cyclic tension-compression at large strain. Int J Plast 2002;18:633–59.

[16] Haddadi H, Bouvier S, Banu M, Maier C, Teodosiu C. Towards an accurate description of the anisotropic behaviour of sheet metals under large plastic deformations: modelling, numerical analysis and identification. Int J Plast 2006;22:2226–71.

[17] Chun B, Jinn J, Lee J. Modeling the Bauschinger effect for sheet metals, part i: theory. Int J Plast 2002;18:571–95.

[18] Cao J, Lee W, Cheng HS, Seniw M, Wang H-P, Chung K. Experimental and numerical investigation of combined isotropic-kinematic hardening behavior of sheet metals. Int J Plast 2009;25:942–72.

[19] Morestin F, Boivin M. On the necessity of taking into account the variation in the young modulus with plastic strain in elastic–plastic software. Nucl Eng Des 1996;162:107–16.

[20] Sun L, Wagoner R. Complex unloading behavior: nature of the deformation and its consistent constitutive representation. Int J Plast 2011;27:1126–44.

[21] Zang S, Liang J, Guo C. A constitutive model for spring-back prediction in which the change of young's modulus with plastic deformation is considered. Int J Mach Tools Manufact 2007;47:1791–7.

[22] Lee J-W, Lee M-G, Barlat F. Finite element modeling using homogeneous anisotropic hardening and application to spring-back prediction. Int J Plast 2012;29:13–41.

[23] Chung K, Lee M-G, Kim D, Kim C, Wenner ML, Barlat F. Spring-back evaluation of automotive sheets based on isotropic-kinematic hardening laws and non-quadratic anisotropic yield functions: Part I: theory and formulation. Int J Plast 2005;21:861–82.

[24] Wang J, Levkovitch V, Reusch F, Svendsen B, Hutink J, van Riel M. On the modeling of hardening in metals during non-proportional loading. Int J Plast 2008;24:1039–70.

[25] Zang S, Guo C, Thuillier S, Lee M. A model of one-surface cyclic plasticity and its application to springback prediction. Int J Mech Sci 2011;53:425–35.

[26] Chung K, Kuwabara T, Verma R, Park T. Numisheet 2011 benchmark 4: pre-strain effect on spring-back of 2d draw bending. In: Huh H, Chung K, Han SS, Chung WJ, editors, The 8th international conference and workshop on numerical simulation of 3D sheet metal forming processes. Seoul, Korea, 2011, pp. 171–175.

[27] Chung K, Park T. Consistency condition of isotropic-kinematic hardening of anisotropic yield functions with full isotropic hardening under monotonously proportional loading. Int J Plast 2013;45:61–84.

[28] Ahn K, Yoo D, Seo M, Park S-H, Chung K. Springback prediction of twip automotive sheets. Metal Mater Int 2009;15:637–47.

[29] Chung K, Lee W, Kim D, Kim J, Chung K-H, Kim C, et al. Macro-performance evaluation of friction stir welded automotive tailor-welded blank sheets: part I—material properties. Int J Solid Struct 2010;47:1048–62.

[30] Kim J, Lee W, Chung K-H, Kim D, Kim C, Okamoto K, et al. Springback evaluation of friction stir welded twb automotive sheets. Metal Mater Int 2011;17:83–98.

[31] Verma RK, Kuwabara T, Chung K, Haldar A. Experimental evaluation and constitutive modeling of non-proportional deformation for asymmetric steels. Int J Plast 2011;27:82–101.

[32] Yoshida F, Uemori T. A model of large-strain cyclic plasticity describing the Bauschinger effect and workhardening stagnation. Int J Plast 2002;18:661–86.

[33] Ziegler H. A modification of Prager's hardening rule. Q Appl Math 1959;17:55–65.

[34] Chaboche JL. Time-independent constitutive theories for cyclic plasticity. Int J Plast 1986;2:149–88.

[35] Firat M. U-channel forming analysis with an emphasis on springback deformation. Mater Des 2007;28:147–54.

[36] Zhang D, Cui Z, Ruan X, Li Y. An analytical model for predicting springback and side wall curl of sheet after U-bending. Comput Mater Sci 2007;38:707–15.

[37] Yamaguchi K, Adachi H, Takakura N. Effects of plastic strain and strain path on Young's modulus of sheet metals. Metal Mater Int 1998;4:420–5.

[38] Lee J-Y, Lee J-W, Lee M-G, Barlat F. An application of homogeneous anisotropic hardening to springback prediction in pre-strained U-draw/bending. Int J Solid Struct 2012;49:3562–72.